Divergence of rodent and primate medial frontal cortex functional connectivity

David J. Schaeffer[a,1], Yuki Hori[a], Kyle M. Gilbert[a], Joseph S. Gati[a], Ravi S. Menon[a,b], and Stefan Everling[a,b]

[a]Centre for Functional and Metabolic Mapping, Robarts Research Institute, University of Western Ontario, London, ON N6A 3K7, Canada; and [b]Department of Physiology and Pharmacology, University of Western Ontario, London, ON N6A 3K7, Canada

Edited by Robert Desimone, Massachusetts Institute of Technology, Cambridge, MA, and approved July 17, 2020 (received for review February 19, 2020)

With the medial frontal cortex (MFC) centrally implicated in several major neuropsychiatric disorders, it is critical to understand the extent to which MFC organization is comparable between humans and animals commonly used in preclinical research (namely rodents and nonhuman primates). Although the cytoarchitectonic structure of the rodent MFC has mostly been conserved in humans, it is a long-standing question whether the structural analogies translate to functional analogies. Here, we probed this question using ultra high field fMRI data to compare rat, marmoset, and human MFC functional connectivity. First, we applied hierarchical clustering to intrinsically define the functional boundaries of the MFC in all three species, independent of cytoarchitectonic definitions. Then, we mapped the functional connectivity "fingerprints" of these regions with a number of different brain areas. Because rats do not share cytoarchitectonically defined regions of the lateral frontal cortex (LFC) with primates, the fingerprinting method also afforded the unique ability to compare the rat MFC and marmoset LFC, which have often been suggested to be functional analogs. The results demonstrated remarkably similar intrinsic functional organization of the MFC across the species, but clear differences between rodent and primate MFC whole-brain connectivity. Rat MFC patterns of connectivity showed greatest similarity with premotor regions in the marmoset, rather than dorsolateral prefrontal regions, which are often suggested to be functionally comparable. These results corroborate the viability of the marmoset as a preclinical model of human MFC dysfunction, and suggest divergence of functional connectivity between rats and primates in both the MFC and LFC.

marmoset | rat | human | resting-state functional MRI | frontal cortex

Despite major differences in the morphology of the rodent and primate brain (size, complexity of convolutions), the cytoarchitecture of the medial frontal cortex (MFC) has been relatively well conserved across these species (1, 2). With a generally comparable MFC structure, rats and mice have been the preferred animal models for preclinical MFC research (3–8). Indeed, rodents are a practicable model that offer ease of housing, low-cost availability, and amenability to genetic manipulation. Nonetheless, it has been suggested that the putative anatomical homologies conserved in rodents do not necessarily represent the same extent of functional equivalence that is found in nonhuman primate models (3, 9, 10). In this study, we examine the increasingly adopted New World common marmoset monkey as an alternative nonhuman primate model for MFC research. Like rodents (and unlike most Old World primates), marmosets are small (~350 g), easily housed, and have a mostly lissencephalic cortex with no cingulate sulcus. Notably, marmosets have a granular lateral frontal cortex (LFC) that is absent in rodents (11).

Across both rodents and primates, MFC can be cytoarchitecturally subdivided into dorsal (area 24) and ventral (areas 25 and 32) components (12–14). The nomenclature often associated with these regions, however, differs across the literature, with prelimbic, infralimbic, and limbic designations of the MFC routinely used to describe these areas in rodents, but rarely so in primates (1, 3). Naming aside, the laminar structure within these areas also shows differences across species. For example, layer IV is present in area 32 of primates (including marmosets), but not in rats (10, 15). Moreover, with rats having a completely agranular cingulate cortex, boundary comparisons with primates are made difficult; the agranular to disgranular boundary used to define boundaries in the MFC of primates is not present in rodents (16–18). To further confound the interpretability of comparative MFC data across rodents and primates, there is some evidence to suggest that although rats do not possess a dorsolateral prefrontal cortex per se (e.g., areas 9, 46, or 47), the rat MFC has "dorsolateral-like" features (19). Such features include connectivity to the mediodorsal thalamus (20) and behavioral equivalency [e.g., working memory for motor responses, memory requiring temporal processing, paired associate learning (21)]. The extent to which these features are functionally analogous, however, has been a point of continuing controversy (3, 9, 10).

Inference of brain homologies across species can be achieved by a variety of methods. Similarities of topographic organization, relative location, architectonic appearance, functional equivalence, and patterns of connectivity can all be used to deduce homology (22). Many of these techniques, including architectonics and histochemical tracing, however, require ex vivo assessment, and thus this information is scarce in humans. As an in vivo technique, MRI allows for circumvention of these constraints by applying similar sequences to index brain structure or function across a variety of different species. Providing functional information across the entire brain, a major advantage of MRI is that it allows for cross-species comparisons both in terms of intrinsic functional organization of a region and also based on

Significance

The question of the whether rodent and primate medial frontal cortex (MFC) share similar functional organization, and whether the rodent medial frontal cortex is functionally analogous to the primate lateral prefrontal cortex (LPFC) is a contentious issue. Here, we probe this long-standing question by comparing whole-brain functional connectivity of the MFC in rodents, nonhuman primates (marmosets), and humans. The results demonstrated a remarkably similar intrinsic functional organization of the MFC across the three species, but clear differences between rodent and primate MFC whole-brain connectivity. Furthermore, in contrast to the common proposal that the rat MFC is functionally analogous with the primate LFC, our results demonstrate clear differences between the rodent MFC and primate LFC interareal functional connectivity.

Author contributions: D.J.S., K.M.G., J.S.G., R.S.M., and S.E. designed research; D.J.S., Y.H., K.M.G., and S.E. performed research; Y.H. contributed new reagents/analytic tools; D.J.S. and Y.H. analyzed data; and D.J.S. wrote the paper.

The authors declare no competing interest.

This article is a PNAS Direct Submission.

[1]To whom correspondence may be addressed. Email: dschaeff@uwo.ca.

This article contains supporting information online at https://www.pnas.org/lookup/suppl/doi:10.1073/pnas.2003181117/-/DCSupplemental.

First published August 17, 2020.

interareal functional connectivity (i.e., connectivity of the rest of the brain with the region in question). "Fingerprinting" is a novel method of comparing interareal connectivity across difference species (23, 24): By comparing the similarity of interareal patterns of connectivity, it is possible to inform functional comparability within the context of embedded networks. In this study, we leveraged our recent developments in ultra high field MRI hardware for small animals (25) to acquire high-quality resting-state

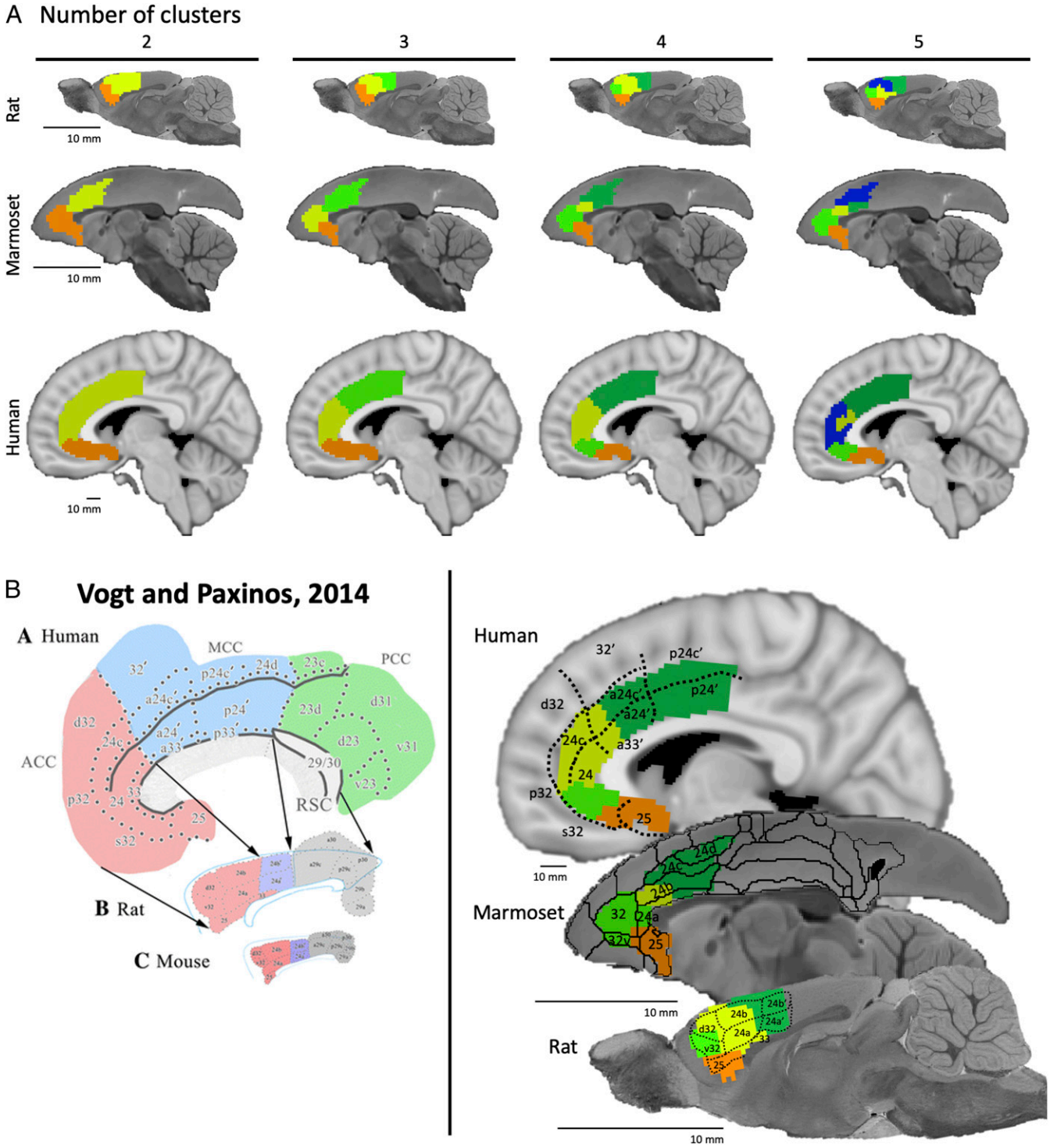

Fig. 1. (*A*) Hierarchical clustering solutions of functional connectivity of MFC in rats (*Top*), marmosets (*Middle*), and humans (*Bottom*). Cluster solutions 2 through 5 (left to right) based on time-course correlations for all three species. Colors indicate separate clusters for each cluster solution. Note that the rat and marmoset brains are increased in scale for ease of display. (*B*) Cluster solutions in each species relative to cytoarchitectonic boundaries. *Left* are the canonical cytoarchitectonic boundaries of MFC in humans and rats (reprinted by permission from ref. 1, Springer Nature: Brain Structure and Function, copyright [2012]), which are superimposed onto the clustering solutions for humans and rats (*Right*). The cytoarchitectonic boundaries superimposed onto the marmoset brain (*Right*) are from the Paxinos et al. marmoset brain atlas (28).

(RS-fMRI) data in rats and marmosets under light anesthesia (at 9.4 Tesla [T]). With the purpose of comparing functional fingerprints, we then compared the rat and marmoset data to high-quality RS-fMRI data in humans from the Human Connectome Project (HCP) database (26).

We applied a data-driven hierarchical clustering approach to intrinsically define the functional boundaries of the MFC in rats, marmosets, and humans, independent of a priori assumptions about the organization of this area (e.g., cytoarchitectonic definitions). Then, we mapped the functional connectivity fingerprints of these newly defined functional clusters with well-defined brain regions extrinsic to both the MFC and lateral prefrontal cortex (LPFC), including the primary auditory cortex (Au1), posterior parietal cortex (PPC), primary somatosensory and motor areas (S1 and M1), amygdala, insula, and striatum. Because rats do not share a number of cytoarchitectonically defined regions of the LPFC with primates (e.g., areas 8, 9, 45, 46, 47), the fingerprinting method also afforded the unique ability to compare between rat MFC and marmoset LPFC, which have often been suggested to be functionally comparable (19).

Results

Intrinsic Functional Clustering. For each species, hierarchical clustering was applied to the functional connectivity values of all voxels within the MFC masks (including areas 25, 24, and 32). The clustering analysis yielded 2 to 20 clusters based on the functional connectivity; solutions 2 through 5 are shown in Fig. 1*A* for rats, marmosets, and humans. As previously described (27), we conducted a silhouette analysis on the marmoset data to determine the optimum number or clusters and found that the optimum number linearly decreased as the solution complexity increased (see figure 1 in ref. 27). Given that hierarchical clustering simply subdivides existing clusters as the cluster number increases (i.e., all cluster solutions are subsets of the two-cluster solution), we also considered whether the seed-based connectivity maps of the subclusters provided additional information when choosing the optimal cluster number. Furthermore, as shown in Fig. 1*B*, the four-cluster solution overlapped relatively well with cytoarchitectonic subdivisions in all three species; this ultimately informed our decision to use conduct further analyses on the four-cluster solution in all three species.

Fingerprint Comparisons. For each species, mean time courses (over space) were extracted from each of the four clusters and functional connectivity was calculated with each voxel and the rest of the brain. The resultant group functional connectivity maps are found in *SI Appendix*, Fig. S2 (rats), *SI Appendix*, Fig. S3 (marmosets), and *SI Appendix*, Fig. S4 (humans). The cosine similarity between the three species was then compared by way of our predefined regions-of-interest (ROIs) (Fig. 2; also shown at the bottom of *SI Appendix*, Figs. S2–S4). As shown in Fig. 3, the cosine similarity metric was highest between marmoset and human interareal connectivity, with cosine similarity values > 0.90 for clusters 1, 2, and 3. The constituent interareal connectivity values for each cluster comparison are shown for all three species in Fig. 3 *A*, *Right*. Permutation testing demonstrated (see Fig. 2*B* for schematic) that the fingerprint comparisons between humans and marmosets were not statistically different for any of the four clusters (Fig. 3), while the fingerprints between humans and rats were different for all four clusters (indicated by cross next to the fingerprint in Fig. 3). The fingerprints between marmosets and rats were also significantly different in clusters 1 and 2 (double cross in Fig. 3). These data suggest that marmosets and humans show greater similarity in terms of MFC interareal connectivity than do rats and humans. Interestingly, however, marmosets and rats showed high cosine similarity in cluster 4; as such, these data suggest that posterior area 24 in marmosets show similarity to both species, with human perhaps showing greater elaboration in this area than marmosets. Indeed, for cluster 4, despite not being statistically different between marmosets and humans, the interareal similarity was more similar to rats than to humans (also not statistically different). Given the differences in cluster 4 between the primate species, we sought to test whether human posterior area 24 (i.e., cluster 4) could be further subdivided in terms of patterns of interareal connectivity (Fig. 3*B*). By systematically seeding 10 regions along this cluster, we found that while some portions of human cluster 4 looked more similar to the marmoset and rat cluster 4 patterns (regions labeled 4, 9, and 10 in Fig. 3*B*), the posterior portion of area 24 in humans seems to be more elaborated, perhaps due to greater areal expansion (29).

The rats were most similar to the primates for cluster 1 (albeit permutation testing showed significant differences from both primate species), which corresponded well to area 25 in all three species. With the exception of the rat–marmoset comparison in cluster 4 (corresponding to posterior area 24), the rats showed progressively less similar interareal connectivity with humans as the clusters moved into areas 32 and 24. This transition was marked by relatively high connectivity with S1 and M1 in the rats, while the primate patterns of connectivity were more heterogeneously distributed across the brain (with the exception of posterior area 24, as described above).

For each species, the interareal patterns of connectivity were also compared with those derived from functional clusters within the marmoset LFC (30). The idea was to inform the hypothesis that the rat MFC is functionally similar to the primate LPFC. When comparing the marmoset MFC to marmoset LFC, there was high similarity of MFC clusters 1 to 3, with LFC clusters 1 to 3 and 6, but not with LPFC clusters 4, 5, and 7. There is high similarity of MFC cluster 4 with LPFC clusters 4, 5, and 7, but little similarity with the most frontal LFC clusters 1 to 3 and 6. Significant differences, as per permutation testing, are shown in Fig. 4, *Left*. Analogous results were found when comparing human MFC–LFC similarity to marmoset MFC–LFC similarity, with the significant cells (Fig. 4) matching the marmoset–marmoset comparison (albeit differences exist when comparing human and marmoset cluster 4). Generally, these results provide evidence that marmosets and humans are functionally analogous both in terms of intrinsic connectivity of the MFC, but also as these patterns relate to marmoset LFC connectivity. This is in sharp contrast to the rats, which showed a different pattern of similarity with marmoset LFC interareal connectivity. In the rats, there was an anterior–posterior shift in similarity (see Fig. 4 for cells with significant differences), in which: cluster 1 was most similar to the frontal pole (LFC clusters 3 and 6); cluster 2 was most similar to LFC cluster 2, 3, and 5; and cluster 3 and 4 were most similar to LFC clusters 4 and 5. Related to Fig. 3*B*, in which we manually subclustered posterior area 24 in the human data, we found further evidence here (Fig. 4) that human cluster 4 seems to be more elaborated than in marmosets, with large differences (all significantly different) between human cluster 4 connectivity and marmoset LFC connectivity. This result, although beyond the scope of this study, warrants further investigation.

Discussion

The question of whether the rodent and primate MFC share similar functional organization and whether the rodent MFC is functionally analogous to the primate LPFC is a contentious issue (31). Here, we compared the intrinsic functional boundaries and interareal connectivity patterns of the MFC (areas 25, 32, and 24) between rats, marmosets, and humans using RS-fMRI data. The results demonstrated a remarkably similar intrinsic functional organization of the MFC across the three species, but also revealed clear differences between rodent and primate interareal patterns of connectivity.

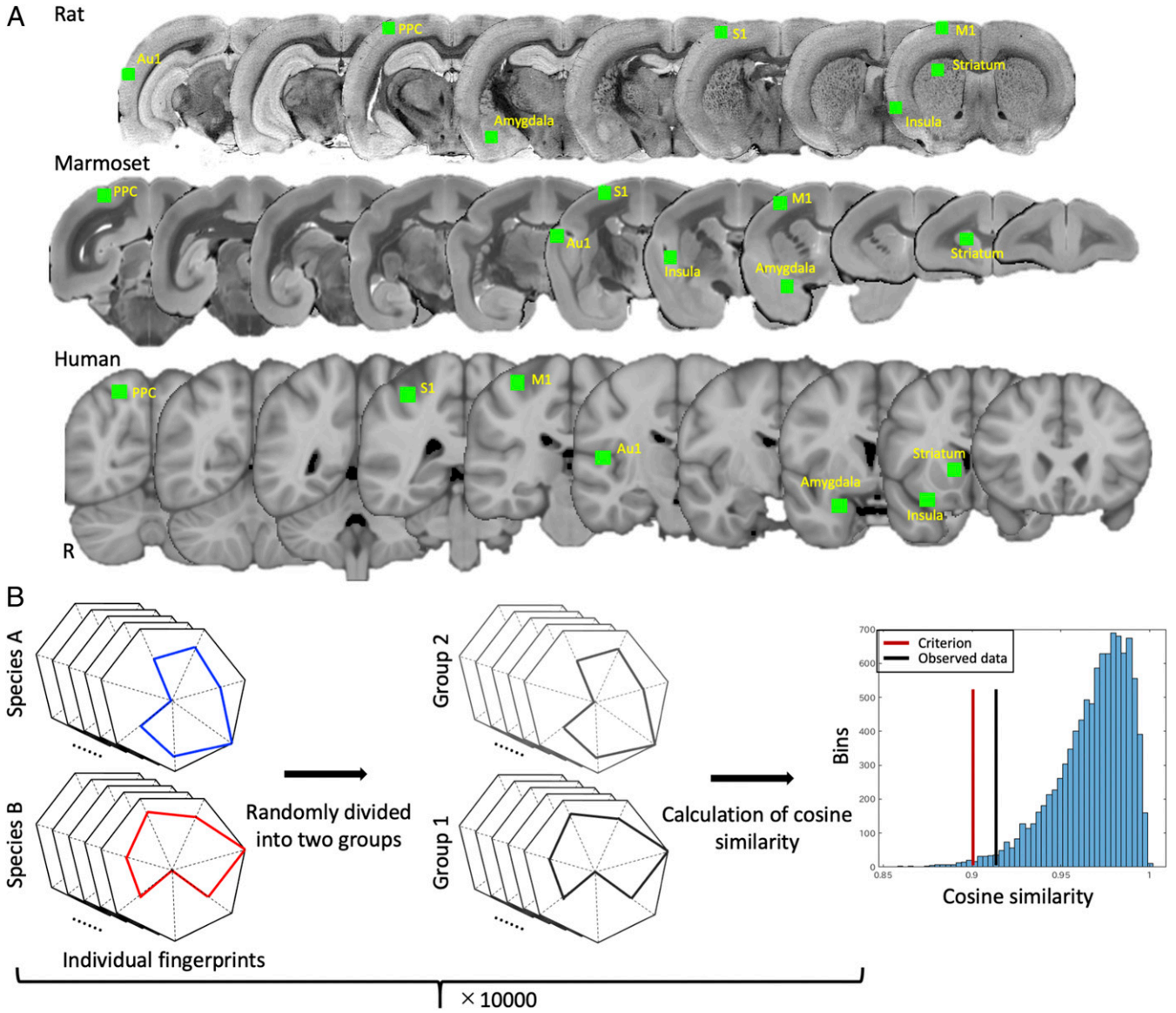

Fig. 2. (*A*) ROI locations for fingerprint analysis. ROIs (all drawn in right hemisphere of respective atlases) are shown in green and overlaid on coronal slices of respective atlas anatomical images for rats (*Top*), marmosets (*Middle*), and humans (*Bottom*). (*B*) Schematic of permutation testing approach used for identifying statistically significant differences between fingerprints. Individual (i.e., scan level) fingerprints of two species were first randomly divided into two groups. Obtained fingerprints in each group were then averaged and normalized to a range of 0 and 1. Cosine similarity was then calculated across species. This process was iterated 10,000 times. The *Right* histogram shows a representative example of the results of permutation testing and shows the distribution of the test statistic, the criterion value (red line), and the observed value given by the data (black line). In this case, actual statistic value was higher than the criterion, indicating no significant differences.

The MFC clusters of the rat brain showed preferential functional connectivity with motor-related regions (M1 and S1), whereas MFC clusters of marmosets and humans showed connectivity more broadly distributed across cortical and subcortical regions. By using the interareal fingerprinting method (24, 32), we also compared the rat MFC and marmoset LFC (30), which are often suggested to be functionally comparable (19, 20). Here, we found that the rat MFC fingerprints showed greatest similarity with premotor LFC regions in the marmoset, rather than dorsolateral prefrontal regions. Overall, these results corroborate the viability of the marmoset as a preclinical model of human MFC dysfunction, and suggest the divergence of functional connectivity between rats and primates in both the MFC and LPFC.

To determine the functional boundaries within the MFC across the three species, we employed a hierarchical clustering approach to compare the group-wise functional connectivity values within the respective MFCs of each species; this approach is well-suited to compare across species, as it is free of any a priori information on where the boundaries may be, thus removing any other rationalizations of cross-species functional comparability (33–36). This technique is not without pitfalls, however, with the user needing to predefine the outer boundaries (i.e., what area to cluster within) based on knowledge of the area, and the number of clusters within the solution being somewhat arbitrary. More detailed subclustering (i.e., more clusters) than that used here may help clarify differences of relative cluster size; for example, note the small size of cluster 3 in marmosets compared to the other species [but see Schaeffer

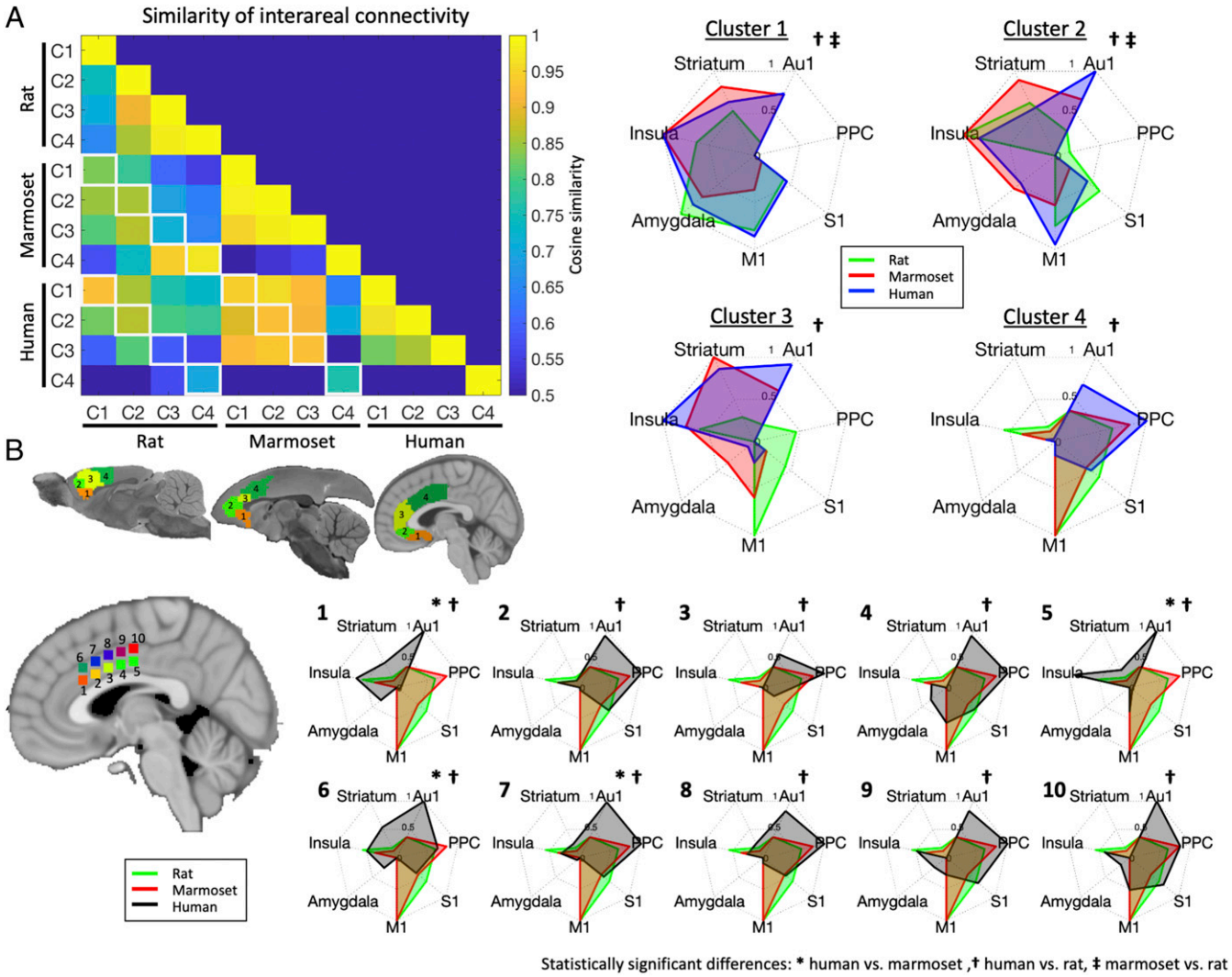

Fig. 3. (*A*) Similarity of interareal functional connectivity across rats, marmosets, and humans. For each species, cosine similarity values are plotted in matrix form (*Left*); cells outlined along diagonals in white show spatially comparable clusters (e.g., cluster 1, C1, corresponding to area 25 between two species). (*Right*) The interareal fingerprint connectivity values contributing to the cosine similarity values in each species, for clusters 1 through 4. Note that for each species, the fingerprints are normalized between 0 and 1 to allow for pattern comparability: A 0 value does not necessarily mean that there was no activation in a region, but just that the region had the lowest relative value within that fingerprint. (*B*) Ten regions systematically subclustered within human cluster 4 compared with rat and marmoset cluster 4; note that subclusters 2, 3, 4, 8, and 9 are similar between humans and marmosets, but 1, 5, 6, and 7 are significantly different, suggesting that human posterior area 24 may be functionally elaborated in humans than in marmosets. Significant differences are marked to the right of each fingerprint.

et al. (27) for evidence that the anterior area 24 cluster shown here may be broken down into two separate functional clusters]. Nonetheless, as shown in Fig. 1, this technique yielded surprisingly consistent functional boundary solutions across the three species. Indeed, we have previously published these cluster solutions in marmosets (27), but functional clustering of the MFC has yet to be compared between rats, marmosets, and humans. As shown in Fig. 1*B*, the four-cluster solution across the three species corresponded strikingly well to the canonical cytoarchitectonic boundaries for each species (1, 28). Although we chose the four-cluster solution for all three species, there is potentially valuable information across other solutions. Ultimately, we found that 1) additional sub clustering did not yield sufficiently distinct interareal patterns of connectivity, and 2) choosing different cluster solutions for each species further confounded comparisons in interareal connectivity. Nonetheless, this data-driven approach suggests that the functional boundaries in the MFC consistently correspond well with the cytoarchitectonic boundaries in both rats and primates.

After separately defining the intrinsic functional clusters of the MFC across the three species, we next sought to compare these clusters in terms of interareal patterns of connectivity. To do so, we compared functional connectivity fingerprints (23, 24, 32) with seven ROIs shared by the three species: Au1, PPC, S1, M1, amygdala, insula, and striatum. Regions within the LFC were purposefully not included (given the lack of similar cytoarchitectonic regions in the rodent brain). Regions of the visual cortices, thalamus, and hippocampus were also not included, given our poor signal quality in those areas in the marmoset or rat RS-fMRI data. These signal disparities are a caveat of imaging small animals in the sphinx position; one alternative may be to develop volumetric phased array radiofrequency coils for imaging these species in the supinated position, or alternatively, in vertical bore MRIs where coil elements can more easily surround the head.

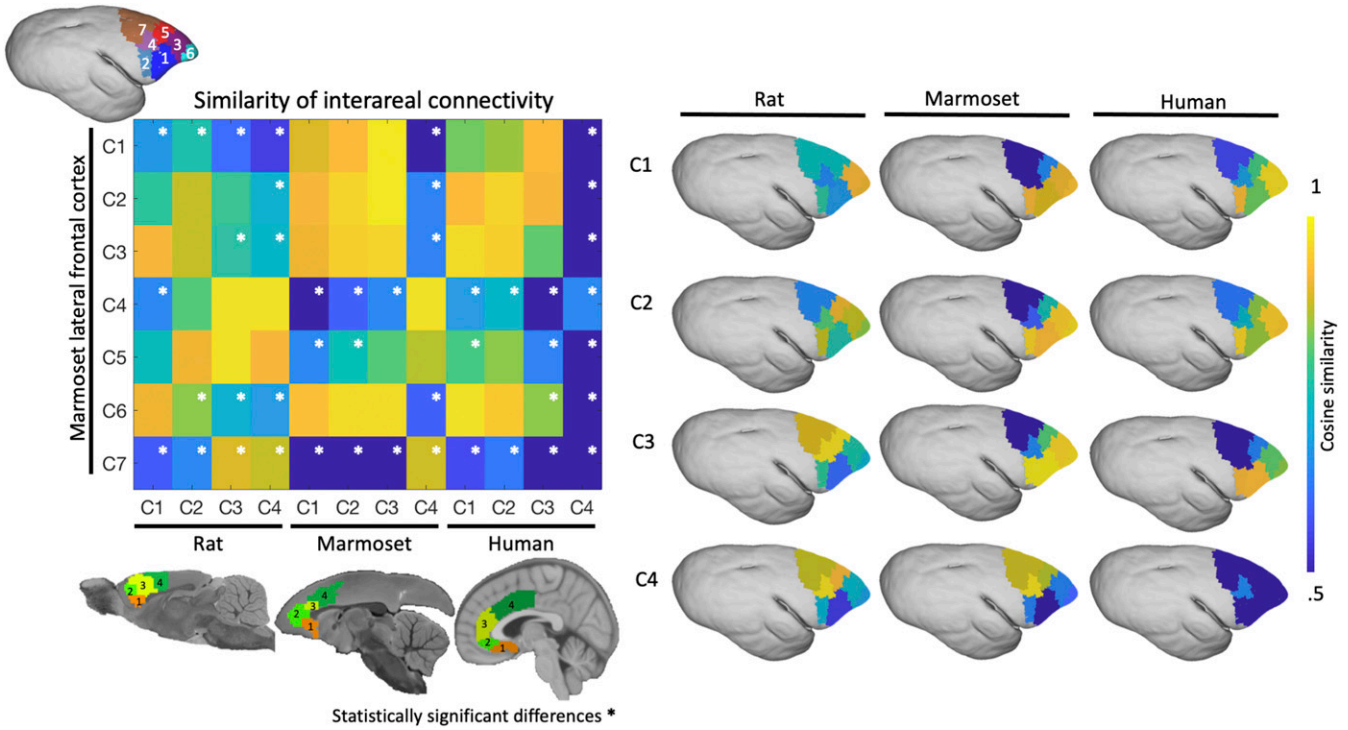

Fig. 4. Similarity of interareal functional connectivity patterns between the MFC (in rats, marmosets, and humans) and LFC connectivity in marmosets (LFC derived from ref. 30). For each species, cosine similarity values are plotted in matrix form (*Left*). (*Right*) The similarity of each species' interareal MFC connectivity with marmoset LFC connectivity; the constituent values are plotted directly on the marmoset LFC. A high cosine similarity value suggests that the connectivity values are more comparable than a lower cosine similarity value. Significant differences are marked by a white asterisk within the similarity matrix (*Left*).

The inclusion of more regions in the fingerprints, specifically subcortical regions, may contribute to a more robust comparison. Still, the marmosets and humans showed more similar patterns of functional connectivity for clusters within areas 25, 32, and 24a (as indexed by cosine similarity) (Fig. 3) than did the comparison between rats and marmosets or rats and humans (which were most dissimilar). Generally, the rats showed progressively less similar interareal connectivity with humans or marmosets as the clusters moved into areas 32 and 24. This transition was marked by relatively high connectivity with the S1 and M1 in the rats, while the primate patterns of connectivity were distributed across the insula, striatum, and Au1 (cluster 3, ~area 24 anterior), then Au1 and PPC (cluster 4, ~area 24 posterior).

One pattern that stands out in contrast to our main finding is that rats and marmosets showed the strongest similarity in cluster 4 (~area 24 posterior), which was different from the human pattern. To delve deeper into this finding, we systematically plotted interareal connectivity for 10 regions within cluster 4 in the humans (as shown in Fig. 3*B*) and found that while some portions of human cluster 4 looked more similar to the marmoset and rat cluster 4 patterns (regions labeled 4, 9, and 10 in Fig. 3*B*), the posterior portion of area 24 in humans seems to be more elaborated than the other species, perhaps due to greater areal expansion (29). Convergent data in macaques suggests that connectivity with motor regions may be highly spatially specific in area 24 (37), which is similar, but perhaps even more elaborated in humans (38). It is also possible that putative differences in cingulate motor areas related to sulcal variability in this middle cingulate area could account for this discrepancy between humans and nonhuman primates (39).

Although anatomical tracing data for the MFC is relatively sparse in marmosets and even more so in humans, our functional connectivity data from rats is consistent with tracing data, with the infralimbic cortex (cluster 1 here) showing strong structural connections with the amygdala and insula (40). Furthermore, the relative distribution of functional connectivity between the MFC and PPC shown here is also similar to evidence from tracer data in rats, with little to no connectivity with the most anterior clusters (41).

Tracing between M1 and area 24 (clusters 3 and 4 here) is also consonant with the functional connectivity data here (42). Interestingly, we did not find strong functional connectivity in the paralimbic cortex (or even more dorsally in the middle cingulate cortex) with the amygdala here, as has been shown by histochemical tracing in rats (40, 43). It could be the case that structural and functional connectivity do not overlap in these regions, or that our fMRI data were not sensitive enough to detect these relationships (amygdala was a relatively low signal-to-noise ratio region; albeit it showed the highest interareal connectivity with cluster 1). For marmosets, we have recently shown relatively good correspondence between RS-fMRI and cellular-based connectivity, but these comparisons were limited to the cortex (44). Some patterns shown here, however, such as connectivity between primate clusters 4 and the amygdala appear to be in contrast to patterns of connectivity found in other primates (45); tracer evidence suggests strongest connectivity between clusters 1 and 4 with the amygdala in macaques (albeit, note that our patterns are relative to the other connections). Indeed, further work is needed to validate the comparability of functional and structural connectivity in all three species; here, however, one of the main motivations of this study was to avoid a priori knowledge of MFC organization/connectivity, and instead to rely only on data-driven functional connectivity.

In addition to comparing interareal connectivity of the MFC between species, we were also interested in how the rat MFC compared to primate LFC connectivity, especially with respect to

the dorsolateral prefrontal cortex. With the common proposal that areas of the rat MFC are functionally analogous with the primate LPFC (19–21, 40), we were interested in framing this question in terms of interareal functional fingerprints. By plotting the rat MFC interareal comparability (indexed by cosine similarity) directly onto the marmoset LFC, we demonstrate that the rat MFC interareal patterns of connectivity show very little similarity to marmoset dorsolateral prefrontal cortex connectivity. In other words, our data do not support the common suggestion that the at MFC is analogous to the dorsolateral prefrontal cortex in primates.

In summary, we present evidence of divergence of functional connectivity in frontal cortices between rodents (rats) and primates. These data demonstrate that although the rat, marmoset, and human show similar intrinsic functional organization within the MFC, the patterns of interareal connectivity are clearly dissimilar between rodents and primates. Taken together, these results suggest that marmosets may be useful nonhuman primate species for MFC function and dysfunction. Indeed, complex behavioral assays are being increasingly implemented in marmosets (46, 47), allowing for modeling of the frontally oriented neurobiological underpinnings of neuropsychiatric disorders; some such protocols (e.g., threat-conditioning paradigms) clearly demonstrate differences in the functional organization of the MFC between rodents and primates (9, 48). As whole-brain connectomic resources become more available across species (e.g., ref. 49), multimodal corroboration, such as that combining both fMRI and cellular level tracing, may offer major inroads into understanding the comparability of topologies between rodents and primates. Although a plethora of information does already exist on structural and functional connectivity within these species, these data are often displayed within the context of a specific question of interest, and thus whole-brain connectivity is not always readily apparent. The ability to consolidate such valuable data and, perhaps more importantly, make these connectivity profiles publicly available (e.g., downloadable topologies in 3D stereotactic space) may be of tremendous use for accelerating the understanding of similarities or differences of connectivity across mammalian species.

Materials and Methods

Subjects.

Marmosets and rats. Data were collected from seven adult marmosets (*Callithrix jacchus*) aged 1 to 6 y weighing from 300 to 500 g, and five adult Wistar rats aged 8 to 12 wk and weighing from 250 to 350 g. Prior to each imaging session, marmoset anesthesia was induced via ketamine at 20 mg/kg; rat anesthesia was induced by placing the animals in an induction chamber with 4 to 5% isoflurane and oxygen with a flow rate between 1 and 1.5 L/min. During scanning, both species were lightly anesthetized with isoflurane and maintained at a level of 1.5% throughout the scan by means of inhalation. Oxygen flow rate was kept between 1.75 and 2.25 L/min throughout the scan. Respiration, SpO_2, and heart rate were continuously monitored via pulse oximeter and were observed to be within the normal range throughout the scans. Body temperature was also measured and recorded throughout, maintained using warm-water circulating blankets, thermal insulation, and warmed air. All animals were head-fixed in stereotactic position using a custom-built MRI bed with ear bars, eye bars (marmosets only), and a palate bar housed within the anesthesia mask (25). Imaging was performed at the Centre for Functional and Metabolic Mapping at the University of Western Ontario. Experimental procedures were in accordance with the Canadian Council of Animal Care policy and protocols approved by the Animal Care Committee of the University of Western Ontario Council on Animal Care. All animal experiments complied with the Animal Research: Reporting of In Vivo Experiments guidelines.

Humans. HCP datasets were used for human comparison analysis (26). High-quality RS-fMRI data for eight subjects (4 scans per subject, 28 scans total; randomly selected) acquired at 3T were used to match the number of scans acquired for the rats and marmosets. These data were preprocessed with the HCP functional pipeline, including motion correction, distortion correction, normalization to Montreal Neurological Institute (MNI) template space, as downloaded from the HCP website (https://www.humanconnectome.org/).

Imaging.

Image acquisition. For both the rats and marmosets, data were acquired on a 9.4 T 31-cm horizontal bore MRI scanner (Varian/Agilent) and Bruker BioSpec Avance III console with the software package Paravision-6 (Bruker BioSpin) and a custom-built high-performance 15-cm-diameter gradient coil with 400-mT/m maximum gradient strength (50). The animal holders and radiofrequency receive arrays were built in-house; the design files for these stereotactic holders have been made open-source (25), with a geometrically optimized phased array receive coil designs for both rats and marmosets. The rat coil was made up of six channels, while the marmoset coil consisted of eight channels, but similar signal-to-noise ratio distributions were achieved with both coils (*SI Appendix*, Fig. S1). Preamplifiers were located behind the animals and the receive coil was placed inside a quadrature birdcage coil (12-cm inner diameter) used for transmission.

For the rats, functional imaging was acquired during one session for each animal, with six functional runs (at 600 volumes each) with the following parameters: Repetition time (TR) = 1,500 ms, echo time (TE) = 15 ms, field-of-view = 38.4 × 38.4 mm, matrix size = 96 × 96, voxel size = 0.4 × 0.4 × 0.4 mm, slices = 35, bandwidth = 280 kHz, GRAPPA (Generalized Autocalibrating Partial Parallel Acquisition) acceleration factor: 2 (anterior–posterior). T2-weighted structural scans were acquired for each animal with the following parameters: TR = 7,000 ms, TE = 44 ms, field-of-view = 38 × 38 mm, matrix size = 192 × 192, voxel size = 0.2 × 0.2 × 0.4 mm, slices = 35.

The marmoset imaging and rat imaging were matched as closely as possible (apart from matrix size), with four to six functional runs (at 600 volumes each) for each marmoset with the following parameters: TR = 1,500 ms, TE = 15 ms, field-of-view = 64 × 64 mm, matrix size = 128 × 128, voxel size = 0.5 × 0.5 × 0.5 mm, slices = 42, bandwidth = 500 kHz, GRAPPA acceleration factor: 2 (anterior–posterior). T2-weighted structural scans were acquired for each animal with the following parameters: TR = 5,500 ms, TE = 53 ms, field-of-view = 51.2 × 51.2 mm, matrix size = 384 × 384, voxel size = 0.13 × 0.13 × 0.5 mm, slices = 42.

For the human subjects, functional runs (at 1,200 volumes each) were acquired with the following parameters at 3T: TR = 720 ms, TE = 33.1 ms, field-of-view = 208 × 180 mm, matrix size = 104 × 90, voxel size = 2 × 2 × 2 mm, slices = 72, bandwidth = 2,290 Hz, acceleration factor: 8 (left–right). T2-weighted structural scans were acquired for each animal with the following parameters: TR = 7,000 ms, TE = 45 ms, field-of-view = 38 × 38 mm, matrix size = 224 × 224, voxel size = 0.17 × 0.17 × 0.75 mm, slices = 45.

Image preprocessing. For both rats and marmosets, data were similarly processed using AFNI (51) and FSL (52). Raw functional images were converted to NifTI format using dcm2niix (53) and reoriented from the sphinx position using FSL. The images were then despiked (AFNI's 3dDespike) and volume registered to the middle volume (AFNI's 3dvolreg). The motion parameters from volume registration were stored for later use with nuisance regression. For the rats, images were smoothed by a 1-mm full-width at half-maximum Gaussian kernel to reduce noise (AFNI's 3dmerge); for marmosets, a 1.5-mm kernel was used. An average functional image was then calculated for each run and registered (FSL's FLIRT) to each animal's T2-weighted image; the 4D time series data were carried over using this transformation matrix. T2-weighted images were manually skull-stripped (including the olfactory bulb in both species) and this mask was applied to the functional images.

T2-weighted images were nonlinearly registered to their respective templates: For rats, images were registered to the anatomical image provided in template space (54). For marmosets, images were registered to the NIH marmoset brain atlas (55). Advanced Normalization Tools (ANTs) (56) was used for nonlinear registration and the resultant transformation matrices were applied to the functional images. The olfactory bulb was manually removed from the T2-weighted images (acquired and template) prior to registration.

As stated above, the human functional images were already preprocessed and registered to MNI template space via the HCP pipeline; in addition, we smoothed the images by a 3.5-mm full-width at half-maximum Gaussian kernel to reduce noise. Functional images from all species were bandpass-filtered between 0.01 and 0.1 Hz.

Intrinsic functional clustering. Once all images were in their respective template spaces, the time-series data were imported into Matlab (The Mathworks) for hierarchical clustering analysis. Explicitly, the clustering solutions for the marmosets were included in our previous publication (27), as were the solutions for the LFC (30), described below. The analysis for the rat and human subjects, however, were unique to this study. Because we were explicitly interested in the MFC, we limited the clustering analysis to areas 24, 25, 32 as defined in rats (54), marmosets (28), and humans (14). Given known differences with human cingulate sulcus anatomy, with the presence or absence of secondary or tertiary paracingulate sulci affecting the anatomical

distribution of the areas of interest, we chose to slightly truncate our human MFC ROI to avoid paracingulate sulci; our mask is nearly identical to that used in previous MRI-based parcellations of the human cingulate (57). Once the masks were created for each species, time courses from each voxel within the MFC masks were extracted for each run and a partial correlation was calculated with each other voxel within the mask (with motion parameters, linear and nonlinear trends, and mean white matter time courses as nuisance regressors). The resultant values were transformed to *z*-scores, then averaged across runs and animals and hierarchical clustering was conducted to extract discrete functional clusters within the MFC mask. Because hierarchical clustering does not require the specification of a number of clusters, we iterated from 2 through 20 cluster solutions (see Fig. 1*A* for 2 through 5 cluster solutions). As described in our previous report (27), a silhouette index was calculated to estimate the optimum number of clusters for our marmoset data (see figure 1 in ref. 27); from these data we chose a cluster solution of four for all three species (see Fig. 1*B* for overlap with respective cytoarchitectonic boundaries).

Fingerprinting. Using four discrete functional clusters derived from each normalized group map (see Fig. 1), seed analyses were conducted between each region (i.e., the mean time course within each cluster) and every other voxel in the brain (with the nuisance regressors described above). A group functional connectivity map (*z*-score map) was then calculated for each of the four clusters for each species. We then specified seven regions extrinsic to both the MFC and LFC in all three species (placement shown in Fig. 2*A*). For each species, ROIs were manually drawn in the Au1, PPC, S1, M1, amygdala, insula, and striatum. Regarding the shape of the ROIs, we used cubes; this approach allowed us to systematically scale the number of voxels contributing to these ROIs with the brain sizes across the species (see Fig. 2*A* for relative scale). Using region-wise ROIs (i.e., cytoarchitectonic boundaries or manual segmentations) would not allow us to control the number of contributing voxels across varying morphologies of regions across species, which differ dramatically in some cases; for example, M1 and M2 in the rat would contribute a much greater proportion of voxels to the analysis than the human or marmoset. Similarly, the parietal cortex proportionally much larger in humans and marmosets than in rats. For the rats, these ROIs were 0.9-mm isotropic cubes, in the marmosets they were 1.6-mm isotropic and in the humans 6-mm isotropic cubes. The placement of the cubes was based on definitions of these areas in the respective atlases, but also (especially in the larger areas) where the peaks of connectivity were in each species; although this might have biased our comparisons, it allowed us to compensate for minor misregistrations. Indeed, we did systematically move these regions around in each species and found that the placement had minimal impact on the overall fingerprint pattern. Despite the potential relevance, we did not place any ROIs in the visual cortex, thalamus, or hippocampus, given the relatively weak signal in our acquisitions in these areas in the rats and primates; the signal would have been overrepresented in the human acquisition (by virtue of using a bird-cage coil) when compared to our rat and marmoset acquisitions, which were acquired in the sphinx position (with the back of the neck preventing coil placement close to the occipital cortices) (*SI Appendix*, Fig. S1). This disparity of signal strength applied to a majority of deep subcortical structures (e.g., hypothalamus, bed nucleus of the stria terminalis) within the marmoset and rat data and, as such, these potentially relevant regions were not included in the fingerprints.

With the seven ROIs defined in each respective species, we then extracted the mean connectivity values within these regions. To compare across the species, we normalized the fingerprint to a range between 0 (weakest connection with any of the target regions) and 1 (strongest connection with any of the target regions). We were thus comparing a pattern of connectivity with target areas, rather than absolute strength in any given species (24). For the comparisons, we calculated the multidimensional cosine similarity across the matrix of functional connectivity fingerprints (24); intuitively similar to a correlation value, the cosine similarity analysis provided an index of how similar or different the interareal fingerprint patterns were. By comparing the cosine of the angle between vectors (i.e., fingerprints), the cosine similarity metric indexes how similar the orientation of a set of vectors are in normalized space, with high similarity values indicating similar fingerprints (i.e., vectors in the same direction) and low scores indicating dissimilar fingerprints (i.e., vectors of diverging direction). By plotting the fingerprints in spider plots (as in Fig. 3) or spatially (as in Fig. 4), we show the specific regions in which the fingerprints differed. We applied this technique to compare rat, marmoset, and human MFC patterns with the seven extrinsic regions and also to the patterns derived from functional clustering of the marmoset LFC [see Schaeffer et al. (30) for details regarding LFC clustering].

Permutation testing was used to test for statistical differences between fingerprints across the species. Permutation tests were performed via in-house code written in Matlab (see Fig. 2*B* for schematic of process). Pairwise comparisons of fingerprints were performed for each cluster by first randomly dividing individual (i.e., scan-level) fingerprints into two groups, group-wise averaging, then normalization of the fingerprints to a range of 0 (weakest connection with any of the target regions) and 1 (strongest connection with any of the target regions). Cosine similarity was then calculated across species. This process was iterated 10,000 times. A value of $P < 0.01$ of the histogram of cosine similarities (e.g., marked "criterion value" on the example histogram in Fig. 2*B*) was considered to be significantly different fingerprints across species.

Data Availability. Data and code are available on GitHub (58). All study data are included in the article and supporting information.

ACKNOWLEDGMENTS. We thank Miranda Bellyou and Lauren Schaeffer for animal preparation and care, and Dr. Alex Li for scanning assistance. Support was provided by the Canadian Institutes of Health Research (FRN 148365) and the Canada First Research Excellence Fund to BrainsCAN. Human data were provided by the Washington University–University of Minnesota Consortium of the Human Connectome Project (WU-Minn HCP; Principal Investigators: David Van Essen and Kamil Ugurbil; 1U54MH091657) funded by the 16 NIH Institutes and Centers that support the NIH Blueprint for Neuroscience Research; and by the McDonnell Center for Systems Neuroscience at Washington University.

1. B. A. Vogt, G. Paxinos, Cytoarchitecture of mouse and rat cingulate cortex with human homologies. *Brain Struct. Funct.* **219**, 185–192 (2014).
2. D. C. Van Essen *et al*., Cerebral cortical folding, parcellation, and connectivity in humans, nonhuman primates, and mice. *Proc. Natl. Acad. Sci. U.S.A.* **116**, 26173–26180 (2019).
3. M. Laubach, L. M. Amarante, K. Swanson, S. R. White, What, if anything, is rodent prefrontal cortex? *Eneuro* **5**, ENEURO.0315-18.2018 (2018).
4. J. M. Hyman, C. B. Holroyd, J. K. Seamans, A novel neural prediction error found in anterior cingulate cortex ensembles. *Neuron* **95**, 447–456.e3 (2017).
5. C. Shaw, J. P. Aggleton, The effects of fornix and medial prefrontal lesions on delayed non-matching-to-sample by rats. *Behav. Brain Res.* **54**, 91–102 (1993).
6. T. J. Bussey, J. L. Muir, B. J. Everitt, T. W. Robbins, Triple dissociation of anterior cingulate, posterior cingulate, and medial frontal cortices on visual discrimination tasks using a touchscreen testing procedure for the rat. *Behav. Neurosci.* **111**, 920–936 (1997).
7. J. K. Seamans, S. B. Floresco, A. G. Phillips, Functional differences between the prelimbic and anterior cingulate regions of the rat prefrontal cortex. *Behav. Neurosci.* **109**, 1063–1073 (1995).
8. T. Steckler, J. L. Muir, Measurement of cognitive function: Relating rodent performance with human minds. *Brain Res. Cogn. Brain Res.* **3**, 299–308 (1996).
9. A. C. Roberts, H. F. Clarke, Why we need nonhuman primates to study the role of ventromedial prefrontal cortex in the regulation of threat- and reward-elicited responses. *Proc. Natl. Acad. Sci. U.S.A.* **116**, 26297–26304 (2019).
10. T. M. Preuss, Do rats have prefrontal cortex? The Rose-Woolsey-Akert program reconsidered. *J. Cogn. Neurosci.* **7**, 1–24 (1995).
11. K. J. Burman, S. M. Palmer, M. Gamberini, M. G. P. Rosa, Cytoarchitectonic subdivisions of the dorsolateral frontal cortex of the marmoset monkey (Callithrix jacchus), and their projections to dorsal visual areas. *J. Comp. Neurol.* **495**, 149–172 (2006).
12. K. Brodmann, *Vergleichende Lokalisationslehre der Grosshirnrinde*, (Johann Ambrosius Barth, Leipzig, 1909).
13. T. Paus, Primate anterior cingulate cortex: Where motor control, drive and cognition interface. *Nat. Rev. Neurosci.* **2**, 417–424 (2001).
14. B. A. Vogt, E. A. Nimchinsky, L. J. Vogt, P. R. Hof, Human cingulate cortex: Surface features, flat maps, and cytoarchitecture. *J. Comp. Neurol.* **359**, 490–506 (1995).
15. K. J. Burman, M. G. P. Rosa, Architectural subdivisions of medial and orbital frontal cortices in the marmoset monkey (Callithrix jacchus). *J. Comp. Neurol.* **514**, 11–29 (2009).
16. D. Ongür, J. L. Price, The organization of networks within the orbital and medial prefrontal cortex of rats, monkeys and humans. *Cereb. Cortex* **10**, 206–219 (2000).
17. C. Fillinger, I. Yalcin, M. Barrot, P. Veinante, Efferents of anterior cingulate areas 24a and 24b and midcingulate areas 24a′ and 24b′ in the mouse. *Brain Struct. Funct.* **223**, 1747–1778 (2018).
18. B. A. Vogt, "Architecture, neurocytology and comparitive organization of monkey and human cingulate cortices" in *Cingulate Neurobiology and Disease*, B. A. Vogt, Ed. (Oxford University Press, 2009), pp. 65–111.
19. H. B. M. Uylings, H. J. Groenewegen, B. Kolb, Do rats have a prefrontal cortex? *Behav. Brain Res.* **146**, 3–17 (2003).
20. J. E. Rose, C. N. Woolsey, Organization of the mammalian thalamus and its relationships to the cerebral cortex. *Electroencephalogr. Clin. Neurophysiol.* **1**, 391–403, discussion 403–404 (1949).

21. R. P. Kesner, Subregional analysis of mnemonic functions of the prefrontal cortex in the rat. *Psychobiology (Austin Tex.)* **28**, 219–228 (2000).
22. L. Krubitzer, The organization of neocortex in mammals: Are species differences really so different? *Trends Neurosci.* **18**, 408–417 (1995).
23. R. E. Passingham, K. E. Stephan, R. Kötter, The anatomical basis of functional localization in the cortex. *Nat. Rev. Neurosci.* **3**, 606–616 (2002).
24. R. B. Mars *et al*., Comparing brains by matching connectivity profiles. *Neurosci. Biobehav. Rev.* **60**, 90–97 (2016).
25. K. M. Gilbert *et al*., Open-source hardware designs for MRI of mice, rats, and marmosets: Integrated animal holders and radiofrequency coils. *J. Neurosci. Methods* **312**, 65–72 (2019).
26. D. C. Van Essen *et al*.; WU-Minn HCP Consortium, The WU-Minn human connectome project: An overview. *Neuroimage* **80**, 62–79 (2013).
27. D. J. Schaeffer *et al*., Intrinsic functional clustering of anterior cingulate cortex in the common marmoset. *Neuroimage* **186**, 301–307 (2019).
28. G. Paxinos, C. Watson, M. Petrides, M. Rosa, H. Tokuno, *The Marmoset Brain in Stereotaxic Coordinates*, (Academic Press, 2012).
29. T. A. Chaplin, H.-H. Yu, J. G. M. Soares, R. Gattass, M. G. P. Rosa, A conserved pattern of differential expansion of cortical areas in simian primates. *J. Neurosci.* **33**, 15120–15125 (2013).
30. D. J. Schaeffer, K. M. Gilbert, J. S. Gati, R. S. Menon, S. Everling, Intrinsic functional boundaries of lateral frontal cortex in the common marmoset monkey. *J. Neurosci.* **39**, 1020–1029 (2019).
31. V. J. Brown, E. M. Bowman, REVIEW rodent models of PFC. *Trends Neurosci.* **25**, 340–343 (2002).
32. R. B. Mars, R. E. Passingham, S. Jbabdi, Connectivity fingerprints: From areal descriptions to abstract spaces. *Trends Cogn. Sci. (Regul. Ed.)* **22**, 1026–1037 (2018).
33. F. X. Neubert, R. B. Mars, A. G. Thomas, J. Sallet, M. F. S. Rushworth, Comparison of human ventral frontal cortex areas for cognitive control and language with areas in monkey frontal cortex. *Neuron* **81**, 700–713 (2014).
34. R. M. Hutchison *et al*., Resting-state connectivity identifies distinct functional networks in macaque cingulate cortex. *Cereb. Cortex* **22**, 1294–1308 (2012).
35. J. Sallet *et al*., The organization of dorsal frontal cortex in humans and macaques. *J. Neurosci.* **33**, 12255–12274 (2013).
36. S. Vijayakumar *et al*., Mapping multiple principles of parietal–frontal cortical organization using functional connectivity. *Brain Struct. Funct.* **224**, 681–697 (2019).
37. R. Dum, P. Strick, Motor areas in the frontal lobe of the primate. *Physiol. Behav.* **77**, 677–682 (2002).
38. N. Picard, P. L. Strick, Motor areas of the medial wall: A review of their location and functional activation. *Cereb. Cortex* **6**, 342–353 (1996).
39. E. Procyk *et al*., Midcingulate motor map and feedback detection: Converging data from humans and monkeys. *Cereb. Cortex* **26**, 467–476 (2016).
40. W. B. Hoover, R. P. Vertes, Projections of the medial orbital and ventral orbital cortex in the rat. *J. Comp. Neurol.* **519**, 3766–3801 (2011).
41. G. M. Olsen *et al*., Organization of posterior parietal-frontal connections in the rat. *Front. Syst. Neurosci.* **13**, 38 (2019).
42. Y. Wang, Y. Matsuzaka, H. Mushiake, K. Shima, Spatial distribution of cingulate cortical cells projecting to the primary motor cortex in the rat. *Neurosci. Res.* **60**, 406–411 (2008).
43. C. J. Reppucci, G. D. Petrovich, Organization of connections between the amygdala, medial prefrontal cortex, and lateral hypothalamus: A single and double retrograde tracing study in rats. *Brain Struct. Funct.* **221**, 2937–2962 (2016).
44. Y. Hori *et al*., Comparison of resting-state functional connectivity in marmosets with tracer-based cellular connectivity. *Neuroimage* **204**, 116241 (2020).
45. H. T. Ghashghaei, C. C. Hilgetag, H. Barbas, Sequence of information processing for emotions based on the anatomic dialogue between prefrontal cortex and amygdala. *Neuroimage* **34**, 905–923 (2007).
46. L. Oikonomidis *et al*., A dimensional approach to modeling symptoms of neuropsychiatric disorders in the marmoset monkey. *Dev. Neurobiol.* **77**, 328–353 (2017).
47. T. Pomberger, C. Risueno-Segovia, Y. B. Gultekin, D. Dohmen, S. R. Hage, Cognitive control of complex motor behavior in marmoset monkeys. *Nat. Commun.* **10**, 1–8 (2019).
48. C. U. Wallis, R. N. Cardinal, L. Alexander, A. C. Roberts, H. F. Clarke, Opposing roles of primate areas 25 and 32 and their putative rodent homologs in the regulation of negative emotion. *Proc. Natl. Acad. Sci. U.S.A.* **114**, E4075–E4084 (2017).
49. P. Majka *et al*., Open access resource for cellular-resolution analyses of corticocortical connectivity in the marmoset monkey. *Nat. Commun.* **11**, 1133 (2020).
50. W. B. Handler *et al*., Design and construction of a gradient coil for high resolution marmoset imaging. *Biomed. Phys. Eng. Express*, 10.1088/2057-1976/ab8d97 (2020).
51. R. W. Cox, AFNI: Software for analysis and visualization of functional magnetic resonance neuroimages. *Comput. Biomed. Res.* **29**, 162–173 (1996).
52. S. M. Smith *et al*., Advances in functional and structural MR image analysis and implementation as FSL. *Neuroimage* **23** (suppl. 1), S208–S219 (2004).
53. X. Li, P. S. Morgan, J. Ashburner, J. Smith, C. Rorden, The first step for neuroimaging data analysis: DICOM to NIfTI conversion. *J. Neurosci. Methods* **264**, 47–56 (2016).
54. G. Paxinos, C. Watson, E. Calabrese, A. Badea, G. Johnson, *MRI/DTI Atlas of the Rat Brain*, (Elsevier, 2015).
55. C. Liu *et al*., A digital 3D atlas of the marmoset brain based on multi-modal MRI. *Neuroimage* **169**, 106–116 (2018).
56. B. B. Avants *et al*., A reproducible evaluation of ANTs similarity metric performance in brain image registration. *Neuroimage* **54**, 2033–2044 (2011).
57. M. Beckmann, H. Johansen-Berg, M. F. S. Rushworth, Connectivity-based parcellation of human cingulate cortex and its relation to functional specialization. *J. Neurosci.* **29**, 1175–1190 (2009).
58. D. Schaeffer, everlingmarmoset: rat_marmoset_human_mfc_clustering. https://github.com/everlingmarmoset/rat_marmoset_human_mfc_clustering. Deposited 14 August 2020.